The Protein Journal, Vol. 26, No. 4, June 2007 (© 2007)
DOI: 10.1007/s10930-006-9069-5

Nanoscopic and Redox Characterization of Engineered Horse Cytochrome *c* Chemisorbed on a Bare Gold Electrode

Laura Andolfi,[1] Paola Caroppi,[2] Anna Rita Bizzarri,[1] Maria Cristina Piro,[2] Federica Sinibaldi,[2] Tommaso Ferri,[3] Fabio Polticelli,[4] Salvatore Cannistraro,[1] and Roberto Santucci[2,5]

In this paper, we exploit the potential offered by site-directed mutagenesis to achieve direct adsorption of horse cyt *c* on a bare gold electrode surface. To this issue, the side chain T102 has been replaced by a cysteine. T102 is close to the surface exposed C-terminal residue (E104), therefore the T102C mutation is expected to generate an exposed cysteine side chain able to facilitate protein binding to the electrode via the sulphur atom (analogously to what observed for yeast iso-1-cyt *c*). Scanning Tunnelling and Tapping Mode Atomic Force Microscopy measurements show that the T102C mutant stably adsorbs on an Au(111) surface and retains the morphological characteristics of the native form. Cyclic voltammetry reveals that the adsorbed variant is electroactive; however, the heterogeneous electron transfer with the electrode surface is slower than that observed for yeast iso-1-cyt *c*. We ascribe it to differences in the tertiary architecture of the two proteins, characterized by different flexibility and stability. In particular, the region where the N- and C-terminal helices get in contact (and where the mutation occurs) is analyzed in detail, since the interactions between these two helices are considered crucial for the stability of the overall protein fold.

KEY WORDS: Atomic force microscopy; cyclic voltammetry; cytochrome *c*; protein engineering; scanning tunnelling microscopy.

1. INTRODUCTION

The control of immobilization and orientation of redox proteins at noble metal surfaces (gold, silver, platinum) is of increasing relevance in biotechnological devices (Castner and Ratner, 2002), including biosensors, biofuel cells, and protein arrays for medical diagnostics (Willner, 2002; Kudera *et al.*, 2001). To assure a suitable electric contact between the molecule and the electrode with minimal perturbation of the macromolecular structure, proteins can be directly immobilized on the metal surface through proper protein linker groups (Willner, 2002); the specific and direct adsorption of redox proteins on a bare metallic surface facilitates a reduced distance between the redox centre and the electrode, thus allowing a rapid heterogeneous electron-transfer (eT) (Marcus and Sutin, 1985). To attain a stable, oriented and spatially-controlled assembling of proteins on a metal surface, the high affinity of native (or engineered) protein disulphides and thiols for noble metals is commonly exploited (Andolfi *et al.*, 2002; Hansen *et al.*, 2003; Heering

[1] Biophysics and Nanoscience Centre, CNISM, Dipartimento di Scienze Ambientali, Università della Tuscia, 01100, Viterbo, Italy.
[2] Dipartimento di Medicina Sperimentale e Scienze Biochimiche, Università di Roma 'Tor Vergata', V. Montpellier 1, 00133, Rome, Italy.
[3] Dipartimento di Chimica, Università di Roma 'La Sapienza', 00185, Rome, Italy.
[4] Dipartimento di Biologia, Università Roma Tre, 00146, Rome, Italy.
[5] To whom correspondence should be addressed. E-mail: santucci@med.uniroma2.it

Abbreviations: cyt *c*, cytochrome *c*; eT, electron-transfer; STM, Scanning Tunnelling Microscopy; TMAFM, Tapping Mode Atomic Force Microscopy.

et al., 2004); as demonstrated, the protein covalently binds to gold via surface side chains containing these groups. An interesting strategy for immobilization on metal of a redox protein missing a specific linking group, consists in introducing one or two cysteine residues into the aminoacidic sequence of the macromolecule, provided that such mutation does not perturb either the protein structure or function (Andolfi *et al.*, 2002; Andolfi *et al.*, 2004).

Horse cytochrome *c* (cyt *c*) is a single chain haemoprotein composed by 104 aminoacidic residues, showing three major and two minor α-helices in the structure. The prosthetic group is covalently bound by two thioether bridges to two cysteine residues, C14 and C17. Under physiological conditions, H18 and M80 are the axial ligands to the haem iron; in particular, M80 plays a primary role for protein activity, since it is thought responsible for the relatively high reduction potential of cyt *c*.

Electrochemistry of soluble horse cyt *c* has been widely investigated and its eT properties well characterized (see, for example, Eddowes and Hill, 1979; Frew and Hill, 1988; Santucci *et al.*, 1991). The protein misses a surface linker able to covalently bind to a gold surface; therefore, nowadays the redox properties of horse cyt *c* directly immobilized on a bare gold electrode have never been reported.

Recent work has demonstrated that yeast iso-1-cyt *c* stably adsorbs on a gold electrode via the exposed C102 residue, and shows a well defined electrochemical activity (Hansen *et al.*, 2003; Bonanni *et al.*, 2003; Heering *et al.*, 2004; Bortolotti *et al.*, 2006). Conversely, equine cyt *c* is electroinactive (Szucs and Novak, 1995; Hill *et al.*, 1997; Zhou *et al.*, 1999) and undergoes aggregation into a flat composite cluster upon contacting the electrode surface (Andersen *et al.*, 1995; Friis *et al.*, 1998), likely because it misses a specific anchoring group for the metal.

In this paper, we exploit the potential offered by site-directed mutagenesis to produce the T102C mutant of equine cyt *c* and investigate the physical and redox properties of the protein chemisorbed onto a Au(111) electrode. The T102C mutation is expected to generate an exposed cysteine side chain able to facilitate binding of the protein to the metal via the –SH group, as observed for yeast iso-1-cyt *c* (Hansen *et al.*, 2003; Heering *et al.*, 2004).

Adsorption of the equine T102C variant on gold has been monitored by high resolution Scanning Tunnelling Microscopy (STM) and Tapping Mode Atomic Force Microscopy (TMAFM) which, thanks to their unprecedent resolution, can detect the (conductive and morphological) properties of the adsorbed protein at level of a single molecule. Data show that the T102C mutant stably adsorbs, as individual molecules, on the Au(111) surface and retains the morphological properties of the native protein. With respect to yeast, the electrode-anchored T102C variant of equine cyt *c* (a schematic view of which is illustrated in Fig. 1) generates a weaker electrochemical signal; the role played by the tertiary structure in affecting the electrochemical behaviour of the chemisorbed protein is analyzed and discussed. Results obtained may have some relevance for the use of cyt *c* in hybrid nanodevices.

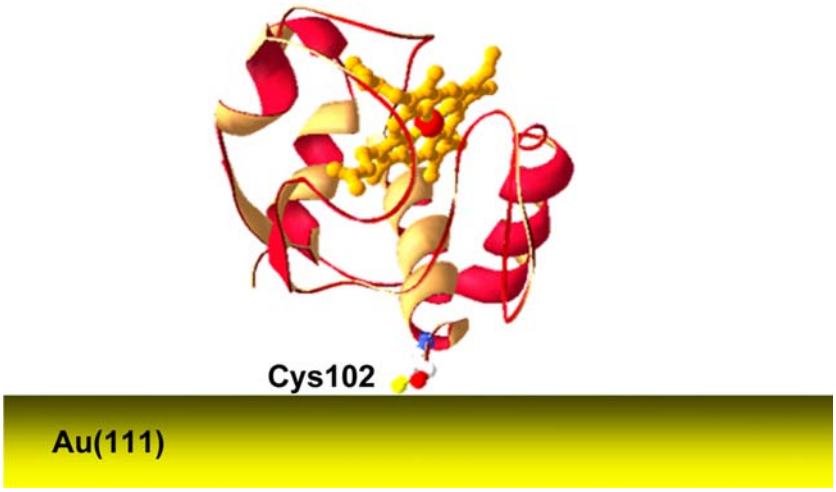

Fig. 1. Schematic representation of the T102C mutant of horse cyt *c* chemisorbed on a bare Au(111) via the C102 sulphur atom.

2. MATERIALS AND METHODS

2.1. Construction of Horse cyt *c* Expression System

A version of the horse cyt *c* synthetic gene was designed on the basis of the sequence of a previously reported cyt *c* synthetic gene (Patel *et al.*, 2001) and its synthesis accomplished by Primm srl (Milano, Italy). The synthetic gene was flanked by the *Nco*I and *Bam*HI restriction sites, at the 5′ and 3′ end, respectively. The pBTRI plasmid (a kind gift of A. Grant Mauk, British Columbia University at Vancouver, Canada) was converted to the horse cyt *c* expression plasmid by removing the yeast iso-1-cyt *c* gene and replacing it with the new synthetic horse cyt *c* gene, by using the unique *Nco*I and *Bam*HI sites. The sequence of the expression construct (pHCyc) was confirmed by the DNA sequence (M-Medical, Milano, Italy). The plasmid pHCyc was then subjected to one round of mutagenesis, which introduced the Thr102Cys substitution into the horse cyt *c* gene.

2.2. Cell Growth and Purification of Recombinant Horse cyt *c*

The expression plasmid of horse cyt *c* was introduced into *E. coli* JM 109 strain; bacterial expression and purification of the recombinant protein were then conducted as previously described (Sinibaldi *et al.*, 2003). Briefly, *E. coli* strain JM 109 containing the pBTRI (or the mutated) plasmid was grown at 37°C, in 2 l of SB medium containing 100 μg/ml ampicillin to an absorbance of 0.3 OD at 600 nm. Induction was accomplished by adding IPTG (isopropyl-ß-D-thiogalactopyranoside) to a final concentration of 0.75 mM. Cells were then incubated at 37°C overnight, harvested by centrifugation and frozen at −80°C. After thawing, the reddish pellets were resuspended in 50 mM Tris–HCl buffer, pH 8.0 (3–4 ml/g of wet cells). Lysozyme (1 mg/ml) and DNase (5 μg/ml) were then added to the homogenized cells. The suspension was left in ice for one hr and then sonicated for 1 min, at medium intensity. After centrifugation, the supernatant was dialyzed overnight against 10 mM phosphate buffer pH 6.2, and loaded on a CM 52 column (40 ml bed volume) equilibrated with the same buffer. Purification was performed by eluting the protein with one volume of 45 mM phosphate pH 6.8, 250 mM NaCl. After purification, the recombinant protein (∼500 μM) had a purity >98% (determined by SDS-PAGE analysis and reverse phase HPLC, not shown) and stored at −80°C in 200 μl aliquots.

2.3. Au(111) Substrates and Sample Preparation

Gold substrates (Arrandee™) with a thickness of 250 nm (±50 nm) were prepared by evaporation on top of an adhesive chromium layer (2.5 nm) deposited on borosilicate substrates. They were annealed with a butane flame to obtain re-crystallized terraces. The quality of the annealed gold surface was assessed by STM, which showed atomically flat (111) terraces over hundreds of nanometers.

The annealed substrates were incubated with 20 μM T102C horse cytochrome *c* in 0.1 M phosphate buffer at pH 7.0, for about 30 min at room temperature. Samples with a lower coverage, facilitating single molecule analysis by Scanning Probe Microscopies, were prepared by reducing the concentration, the incubation time and the temperature (down to 4°C). After incubation samples were then rinsed with ultrapure water (Milli Q, 18.2 MΩ), blown dry with pure nitrogen and immediately imaged by Scanning Probe Microscopies.

2.4. STM Imaging

STM measurements were performed in constant current mode using a Picoscan system (Molecular Imaging) equipped with a 10 μm scanner with a final preamplifier sensitivity of 1 nA/V. The imaging was performed in ultrapure water. STM tips were made from PtIr (80:20) by electrochemical etching of a 0.25 mm wire in a melt of $NaNO_3$ and NaOH. Tips were then insulated with molten Apiezon wax. Only tips displaying leakage levels below 10 pA were used for imaging.

2.5. AFM Imaging

AFM images were acquired by a NanoscopeIIIa/Multimode scanning probe microscope (Digital Instruments) equipped with a 12 μm scanner. TMAFM imaging was performed in ultrapure water. The free oscillation of the cantilever was set to approximately 1.5 V; after engaging, the set point was adjusted to minimize the applied force.

Oxide-sharpened silicon nitride probes (Digital Instruments), 85 μm long, with nominal radius of curvature of less than 20 nm and spring constants of 0.50 Nm/m were used.

2.6. Electrochemical Measurements

Voltammetric measurements were carried out at 25°C in a glass microcell (sample volume: 1 ml) equipped with a reference calomel electrode (E = 244 mV vs NHE, at 25°C; Amel, Milan, Italy), a Pt wire as the counter-electrode and a gold disk electrode (2 mm diameter) as the working electrode. An Amel 433/W multipolarograph (Milan, Italy) interfaced with a PC, was employed for electrochemical measurements. Before the experiment, the solution was deaerated for 30 min by a gentle flow of pure nitrogen maintained just above the solution surface.

Adsorption of the protein on the gold electrode was achieved directly in the electrochemical cell by dipping the electrode in 1 ml of a 0.1 mM T102C horse ferrous cyt *c* solution (solvent composition: 10 mM phosphate buffer, pH 7.0, containing 50 mM $KClO_4$) for 15–16 hr at 5°C. The reduction of T102C ferric cyt *c*, necessary because the oxidized protein undergoes partial dimerization, was obtained by adding 1,4 dithiotreitol in solution. Reductant excess was then removed by eluting the protein solution on a Sephadex PD10 column (Amersham Biosciences).

3. RESULTS AND DISCUSSION

At 25°C and neutral pH, the T102C mutant of horse cyt *c* displays circular dichroism and electronic absorption spectra (not shown) unchanged with respect to the native protein. In particular, the variant displays the 695-nm absorbance band, considered a probe for the integrity of the native M80-Fe(III) axial coordination (Stellwagen and Cass, 1974). This indicates that the T102C mutation does not perturb the tertiary architecture of the protein.

3.1. STM and TMAFM Measurements

As schematically shown in Fig. 1, the T102C mutation is expected to facilitate protein binding to gold via the –SH group of C102, analogously to what observed for yeast iso-1-cyt *c* (Hansen *et al.*, 2003; Bonanni *et al.*, 2003; Heering *et al.*, 2004; Bortolotti *et al.*, 2006). A combination of STM and TMAFM was used to characterize the protein variant adsorbed on Au(111) at the single-molecule level. The extent of protein adsorption on Au(111) was controlled by choosing appropriate parameters for protein incubation, as well as protein concentration, time and temperature (down to 4°C). To facilitate single molecule analysis both in STM and TMAFM images a low protein coverage was achieved. Figure 2 shows a STM image where single molecules of the ferric T102C mutant are clearly

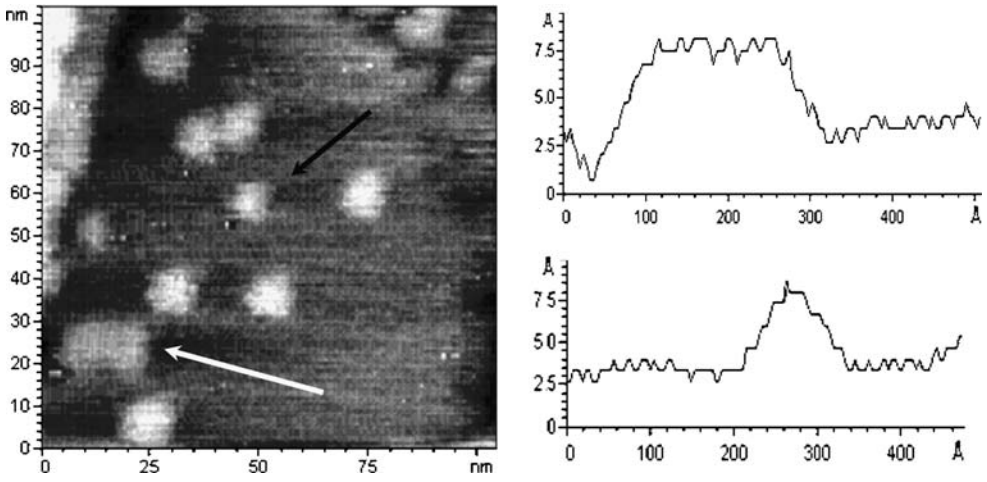

Fig. 2. Constant current STM image of the T102C mutant of horse ferric cyt *c* immobilized on a Au(111) surface. Tunneling current 50 pA, bias voltage 0.6 V, scan rate 3.3 Hz. Cross section profile of the molecule indicated by the white arrow is shown in the upper part of the lateral panel, while cross section profile of the molecule indicated by the black arrow is shown in the lower part of the lateral panel.

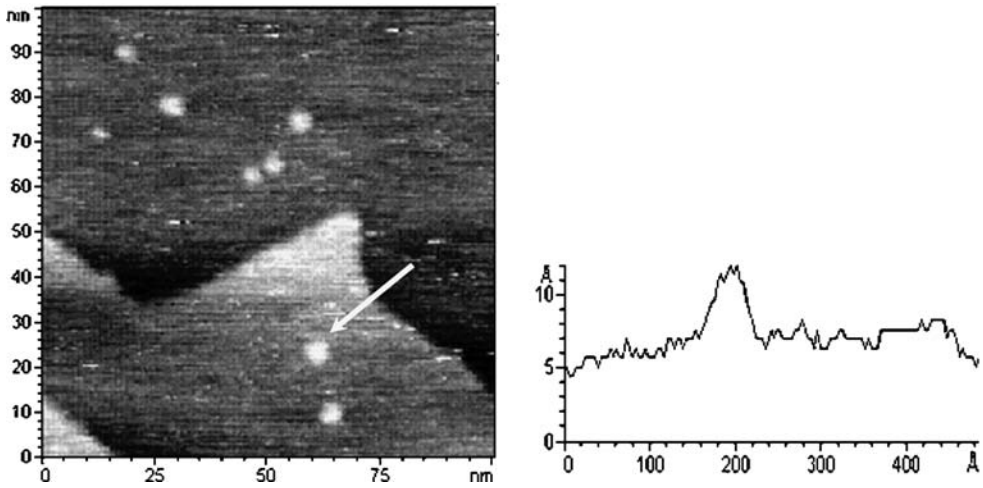

Fig. 3. Constant current STM image of the T102C mutant of horse cyt *c* immobilized on Au(111) surface, after reduction with 1,4 dithiothreitol. Tunneling current 50 pA, bias voltage 0.6 V, scan rate 2.8 Hz. Cross section profile of the molecule indicated by the white arrow is reported in the lateral panel.

discernible. The images are very reproducible and the molecules are not swept away upon repetitive scans; this indicates that the equine variant strongly binds to gold, and that a stable electric contact between the protein and the gold electrode is likely established. Analysis of the STM images' lateral size shows that some molecules (see the black arrow in Fig. 2) have an almost circular shape with a lateral size of about 5 nm (a value close to what expected from crystallography). At variance, other molecules (see the white arrow in Fig. 2) reveal an almost elliptical shape and a lateral size of about 9–10 nm. Both molecule populations remain stable after repetitive scans, consistent with a strong binding to Au(111). We assume that the molecules with 10 nm-lateral size are dimers that adsorb on Au(111) via the intermolecular disulphide group. Such a hypothesis is confirmed by the fact that protein reduction by 1,4-dithiothreitol gives rise to a homogeneous molecular coverage on gold characterized, as shown in Fig. 3, by molecules with lateral size of 4.0 ± 0.8 nm (i.e., monomers), in full agreement with the expected crystallographic value.

For what concerns the vertical size, we measured an almost homogeneous dimension which, however, is considerably reduced (< 1 nm) respect to what expected for the adsorbed variant on Au(111). This is a recurrent feature in STM images acquired on redox proteins and biological material in general (Bonanni *et al.*, 2004; Alliata *et al.*, 2004; Davis *et al.*, 2004), and has been more closely addressed in a previous work dealing with the question about recovering of the real vertical size of proteins by STM (Davis *et al.*, 2004).

To gain a deeper insight into the protein morphology (particularly concerning the height over Au(111) which, as mentioned above, is not recovered in STM), an analysis by TMAFM was performed. The AFM images of the Au(111)-adsorbed ferrous T102C mutant are stable and reproducible even after repetitive scans; this confirms that the protein strongly binds to gold. As shown in the high-resolution image of Fig. 4, single molecules appear well resolved on the gold substrate; a representative cross section of a single T102C molecule is shown in the lateral panel of the figure.

The molecule height on the gold surface has been estimated from an analysis of the cross section profiles relative to one hundred molecules of the T102C variant. This provides a statistical distribution of the protein vertical size resulting in the histogram shown in Fig. 5. The mean height of the T102C mutant molecules on gold is 2.6 nm (standard deviation: 0.8 nm); such a value is in good agreement with X-ray crystallographic data, and finds a satisfactory correspondence with the value found for yeast iso-1-cyt *c* adsorbed on Au(111) (Bonanni *et al.*, 2003). This suggests that, when adsorbed on Au(111), the equine T102C mutant arranges on the metal surface similarly to yeast iso-1-cyt *c*.

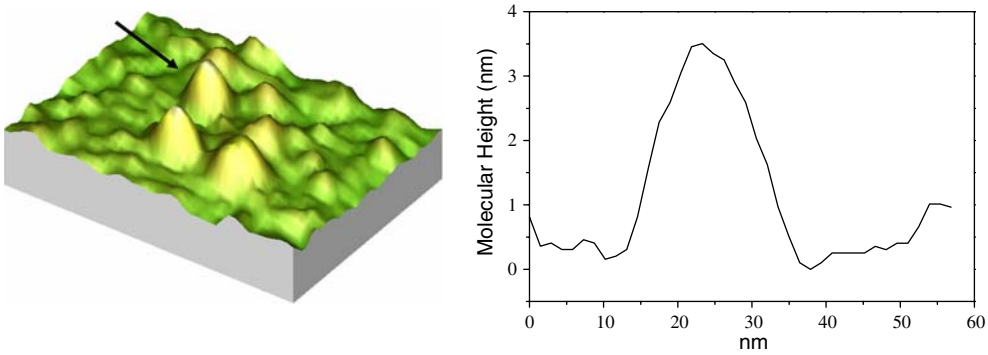

Fig. 4. Three-dimensional view of a TMAFM image of T102C molecules adsorbed on Au(111), recorded in ultra-pure water representative cross-section profile, recorded along the molecule indicated by the white arrow, is shown in the lateral panel.

3.2. Cyclic Voltammetry Measurements

Electrochemistry of the ferrous T102C equine mutant chemisorbed at a naked gold electrode was investigated at neutral pH and 25°C. The variant was studied in the reduced form, which homogeneously chemisorbs on Au as a monomer (Fig. 2). In ferrous cyt *c*, in fact, the reactive -SH group of C102 lies buried within a hydrophobic region and the dimerization process, due to formation of a disulfide bond between two monomers, would require significant conformational changes in the C-terminal helix of the macromolecule (Louie *et al.*, 1988). Figure 6 shows the cyclic voltammogram of the chemisorbed protein run at 10 mV/s. The voltammogram appears defined and characterized by two waves with a i_{pc}/i_{pa} ratio of approx. 0.6, indicating quasi-reversibility. As for chemisorbed yeast cyt *c* (Heering *et al.*, 2004), a peak separation (ΔEp = 105 mV) is observed. The calculated redox potential, $E_{1/2}$ = 255(±5) mV vs the normal hydrogen electrode (NHE), is in excellent agreement with the value reported in the literature for soluble equine cyt *c* (see, for example, Eddowes and Hill, 1979; Santucci *et al.*, 1991). These data suggest that the chemisorbed protein remains folded, the haem lies buried inside the protein matrix, and the native M80-Fe axial coordination is retained (Senn and Wuthrich, 1985; Ferri *et al.*, 1996); when exposed to the solvent, in fact, the haem generates a voltammetric signal at lower potential, $E_{1/2} \sim -160$ mV vs NHE, under the conditions investigated (Santucci *et al.*, 1988; Bianco *et al.*, 1990; Santucci *et al.*, 2000). Unlike yeast (Heering *et al.*, 2004), the voltammetric signal of horse cyt *c* is lost at scan rates higher than 20 mV/s, consistent with a slower interfacial eT rate. As shown in the figure, the signal is significantly improved in the presence of soluble ferrous cyt *c*. In this case, the voltammogram is characterized by two waves with a i_{pc}/i_{pa} ratio of approx. 0.85 and the peak separation (ΔEp = 58 mV) is almost identical to the theoretical value expected for a fully reversible one-electron-transfer reaction (57 mV, at 25°C) relative to soluble systems. Also the calculated redox potential, $E_{1/2}$ = 250(±5) mV vs the normal hydrogen electrode (NHE), is in good agreement with the value reported in the literature

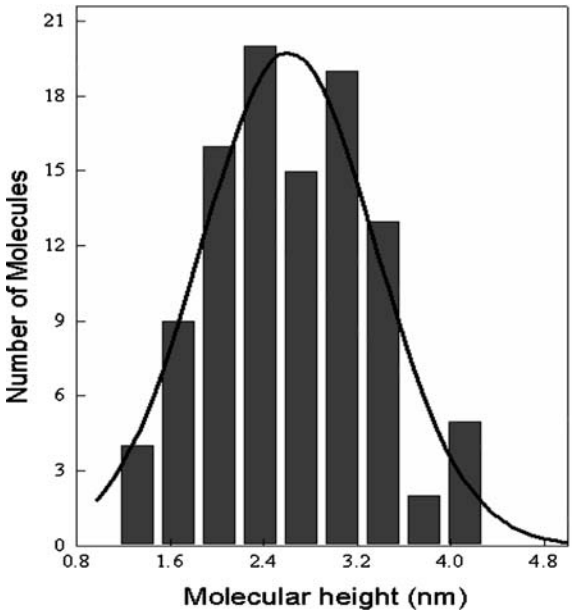

Fig. 5. Statistical analysis of T102C molecular height on bare Au(111) surface. The vertical dimension of the proteins was estimated from individual cross-section analysis of 100 molecules. The mean height is 2.6 nm, with a standard deviation of 0 .8 nm.

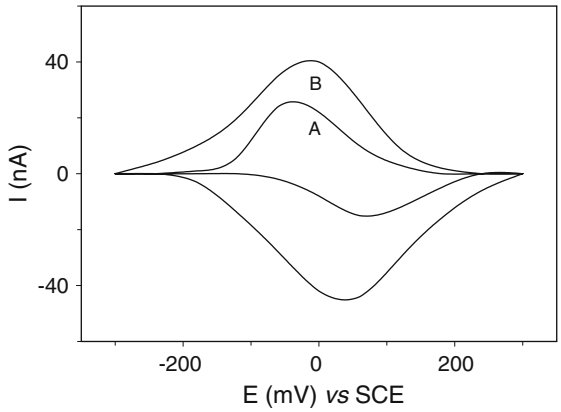

Fig. 6. Dc cyclic voltammetry of the T102C mutant of horse ferrous cyt *c* chemisorbed on a gold electrode. Voltammograms illustrated were run in the absence (A) and in the presence (B) of soluble (0.1 mM) T102C ferrous cyt *c*. Scan rate: 10 mV/s. Experimental conditions: 10 mM phosphate buffer, pH 7.0, containing 50 mM $NaClO_4$. The temperature was 25°C. Adsorption of the protein onto the Au electrode was achieved by dipping the electrode into a 0.1 mM protein solution for 15–16 hr at 5°C. Voltammograms illustrated are subtracted of the background current.

(Eddowes and Hill, 1979; Santucci *et al*., 1991). This suggests that the adsorbed protein facilitates eT between soluble cyt *c* and the electrode; in other words, it acts as electrochemical mediator.

3.3. Structural Analysis of Helix–Helix Interaction

The weaker electroactivity of equine T102C cyt *c* with respect to yeast reasonably reflects conformational differences in the two proteins, in despite of their apparently close tertiary structure (Bushnell *et al*., 1990; Louie and Brayer, 1990; Banci *et al*., 1997a; Banci *et al*., 1997b). It is well known, for instance, that horse cyt *c* possesses a more rigid tertiary architecture and higher stability (Lett *et al*., 1999). The insertion of a cysteine, in place of a threonine, at position 102 occurs in the region formed by the C- and N-terminal helices, stabilized by cross-link interactions between the two helical segments. This region provides a fundamental contribution to the overall protein stability (Colon *et al*., 1996; Rumbley *et al*., 2001); thus, it becomes crucial defining if the slower heterogeneous eT rate of horse cyt *c* is to be imputed to the marked rigidity of the (C- and N-) terminal helices region.

To shed light on this point, a comparative analysis of the three-dimensional structure of horse and yeast cyt *c* was undertaken. In particular, we analyzed the structural organization in the region where the N- and C-terminal helices get in contact. Important differences were found. This is intriguing because, as said, interactions between the two helices are crucial for the stability of the overall protein fold (Lett *et al*., 1999). As illustrated in Fig. 7A, the helix–helix interaction in horse cyt *c* is mainly mediated by very strong charge–charge interactions involving the N-terminal amino group and the side chains of

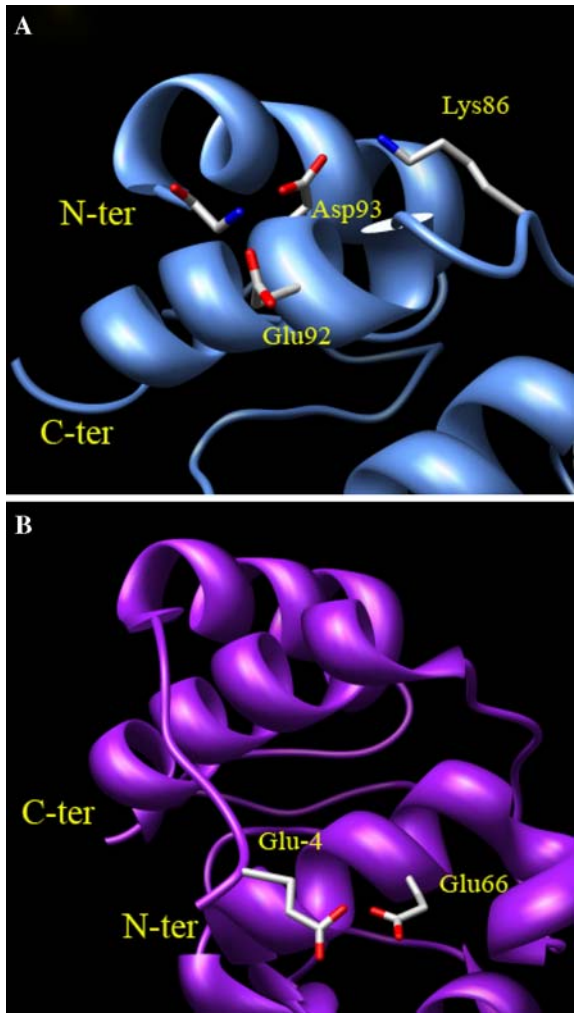

Fig. 7. (A) Schematic representation of the three-dimensional structure of horse cyt *c* (PDB code 1AKK (Bushnell *et al*., 1990)) showing the protein region in which the N- and C-terminal helices contact each other. Note the charge network involving the N-terminal amine group and K86, E92 and D93. (B) Corresponding region of yeast iso-1-cyt *c* three-dimensional structure (PDB code 1YCC (Louie and Brayer, 1990)). Note the unstructured N-terminal extension and the unfavourable charge–charge interaction between E-4 and E66. The figure was made with Chimera (available at http://www.cgl.ucsf.edu/chimera).

residues E92 and D93 (Louie and Brayer, 1990). D93 in turn is hold in place by a strong salt bridge involving K86. The measured distance among groups forming this charge network, approx. 2.6 Å in all cases (thus, well below the threshold usually assumed for strong salt bridges), confirms the hypothesis of strong interactions between the two helices. Additional stability is furtherly provided by the hydrophobic interactions among F10, L94 and L98.

The charge complementarity described above for horse cyt *c* is not observed in yeast. As shown in Fig. 7B, the N-terminal region of yeast cyt *c* displays an unstructured extention (residues −1 to −5; (Banci *et al.*, 1997a) and the N-terminal helix contacts the C-terminal region mainly through hydrophobic interactions which involve residues F10, L94 and L98 (an additional source of instability is represented also by the unfavourable charge–charge interaction between residues E-4 and E66, located at approx. 6 Å one from the other; see the figure). Thus, it is likely that the higher flexibility of the helix-helix region in yeast cyt *c* facilitates the chemisorbed protein to get a proper orientation favouring rapid electron exchange with the metal surface.

4. CONCLUSIONS

The present study demonstrates that the T102C mutant of equine cyt *c* stably adsorbs on bare gold, as a monomer in the reduced state and as a monomer–dimer mixture in the oxidized state. The morphological features of the adsorbed protein are in good accord with crystallographic values and resemble those of yeast iso-1-cyt *c*. This suggests that the two Au-bound proteins retain a compact conformation, and that the adsorption process involves in both cases the sulphur of residue C102. Also, both proteins remain strongly bound to the metal. Unlike yeast, equine cyt *c* generates a weak electrochemical signal, indicative of a slower heterogeneous eT rate with the electrode surface. This may be attributed to the fact that, unlike yeast, horse cyt *c* undergoes dramatic conformational changes when changing its oxidation state (Qi *et al.*, 1996; Banci *et al.*, 1997a); in addition, we identify in the marked rigidity of the helix–helix interface another factor responsible for the low electroactivity of the equine protein. Finally, results here described may have some relevance for utilization of cyt *c* in hybrid nanodevices.

ACKNOWLEDGMENTS

Research funded in part by grants from Italian MIUR (PRIN 2004 055484). L. Andolfi acknowledges the Research Grant ''Rientro dei Cervelli'' from MIUR.

REFERENCES

Alliata, D., Andolfi, L., and Cannistraro, S. (2004). *Ultramicroscopy* **101:** 231–240.
Andersen, J. E. T., Møller, P., Pedersen, M. V., and Ulstrup, J. (1995). *Surf. Sci.* **325:** 193–205.
Andolfi, L., Cannistraro, S., Canters, G. W., Facci, P., Ficca, A. G., Van Amsterdam, I. M. C., and Verbeet, M. Ph. (2002). *Arch. Biochem. Biophys.* **399:** 81–88.
Andolfi, L., Bruce, D., Cannistraro, S., Canters, G. W., Davis, J. J., Hill, H. A. O., Crozier, J., Wrathmell, C. L., and Astier, Y. (2004). *J. Electroanal. Chem.* **565:** 21–28.
Banci, L., Bertini, I., Bren, K. L., Gray, H. B., Sompornpisut, P., and Turano, P. (1997a). *Biochemistry* **36:** 8992–9001.
Banci, L., Bertini, I., Gray, H. B., Luchinat, C., Reddig, T., Rosato, A., and Turano, P. (1997b). *Biochemistry* **36:** 9867–9877.
Bianco, P., Haladjian, J., and Draoui, K. (1990). *J. Electroanal. Chem.* **279:** 305–314.
Bonanni, B., Alliata, D., Bizzarri, A. R., and Cannistraro, S. (2003). *Chem. Phys. Chem.* **4:** 1183–1188.
Bonanni, B., Alliata, D., Andolfi, L., Bizzarri, A. R., and Cannistraro, S. (2004). In: Norris, C. P. (ed.), *Surface Science Rersearch Development*, Nova Science Publishers Inc, New York, pp 1–73.
Bortolotti, C. A., Battistuzzi, G., Borsari, M., Facci, P., Ranieri, A., and Sola, M. (2006). *J. Am. Chem. Soc.* **128:** 5444–5451.
Bushnell, G. W., Louie, G. V., and Brayer, G. D. (1990). *J. Mol. Biol.* **214:** 585–595.
Castner, D. G., and Ratner, B. D. (2002). *Surf. Sci.* **500:** 28–60.
Colon, W., Elove, G. A., Wakem, L. P., Sherman, F., and Roder, H. (1996). *Biochemistry* **35:** 5538–5549.
Davis, J. J., Morgan, D. A., Wrathmell, C. L., and Zhao, A. (2004). *IEE Proc-Nanobiotechnol.* **151:** 37–47.
Eddowes, M. J., and Hill, H. A. O. (1979). *J. Am. Chem. Soc.* **101:** 4461–4464.
Ferri, T., Poscia, A., Ascoli, F., and Santucci, R. (1996). *Biochim. Biophys. Acta* **1298:** 102–108.
Frew, J. E., and Hill, H. A. O. (1988). *Eur. J. Biochem.* **172:** 261–269.
Friis, E. P., Andersen, J. E. T., Madsen, L. L., Møller, P., Nichols, R. J., Olesen, K. G., and Ulstrup, J. (1998). *Electrochim. Acta* **43:** 2889–2897.
Hansen, A. G., Boisen, A., Nielsen, J. U., Wackerbarth, H., Chorkendorff, I., Andersen, J. E., Zhang, J., and Ulstrup, J. (2003). *Langmuir* **19:** 3419–3427.
Heering, H. A., Wiertz, F. G., Dekker, C., and de Vries, S. (2004). *J. Am. Chem. Soc.* **126:** 11103–11112.
Hill, H. A. O., Hunt, N. I., and Bond, A. M. (1997). *J. Electroanal. Chem.* **436:** 17–25.
Kudera, M., Hill, H. A. O., Dobson, P. J., Leigh, P. A., and William, S. (2001). *Sensors* **1:** 18–28.
Lett, C. M., Rosu-Myles, M. D., Frey, H. E., and Guillemette, J. G. (1999). *Biochim. Biophys. Acta* **1432:** 40–48.
Louie, G. V., and Brayer, G. D. (1990). *J. Mol. Biol.* **214:** 527–555.
Louie, G. V., Hutcheon, W. L., and Brayer, G. D. (1988). *J. Mol. Biol.* **199:** 295–314.

Marcus, R. A., and Sutin, N. (1985). *Biochim. Biophys. Acta* **811:** 265–322.
Patel, C. N., Lind, M. C., and Pielak, G. (2001). *Protein Expr. Purif.* **22:** 220–224.
Qi, P. X., Beckman, R. A., and Wand, A. J. (1996). *Biochemistry* **35:** 12275–12286.
Rumbley, J., Hoang, L., Mayne, L., and Englander, S. W. (2001). *Proc. Natl. Acad. Sci. (USA)* **98:** 105–112.
Santucci, R., Reinhard, H., and Brunori, M. (1988). *J. Am. Chem. Soc.* **110:** 8536–8537.
Santucci, R., Faraoni, A., Campanella, L., Tranchida, G., and Brunori, M. (1991). *Biochem. J.* **273:** 783–786.
Santucci, R., Fiorucci, L., Sinibaldi, F., Polizio, F., Desideri, A., and Ascoli, F. (2000). *Arch. Biochem. Biophys.* **379:** 331–336.
Senn, H., and Wuthrich, K. (1985). *Q. Rev. Biophys.* **18:** 111–134.
Sinibaldi, F., Piro, M. C., Howes, B. D., Smulevich, G., Ascoli, F., and Santucci, R. (2003). *Biochemistry* **42:** 7604–7610.
Stellwagen, E., and Cass, R. (1974). *Biochem. Biophys. Res. Comm.* **60:** 371–375.
Szucs, A., and Novak, M. (1995). *J. Electroanal. Chem.* **383:** 75–84.
Willner, I. (2002). *Science* **298:** 2407–2408.
Zhou, Y., Nagaoka, T., and Zhu, G. (1999). *Biophys. Chem.* **79:** 55–62.